

Quantifying farmed kelp atmospheric CO₂ uptake through localized air-sea flux in the Northern Gulf of Alaska

Josianne Haag¹, Cale A. Miller², Jonah Jossart¹, Amanda L. Kelley¹

¹College of Fisheries and Ocean Sciences, University of Alaska Fairbanks, Fairbanks, AK, 99775, USA

5 ² Department of Earth Sciences, Geosciences, Utrecht University, 3508 TC, The Netherlands

Correspondence to: Josianne Haag (jhaag6@alaska.edu)

Abstract. The rapid growth of mariculture in the United States, particularly in Alaska, has ignited interest in the co-benefit of using farmed kelp as a mitigation strategy against anthropogenic carbon dioxide (CO₂) released to the atmosphere. Here, we quantified the air-sea CO₂ flux in ~~three-two~~ kelp farms ~~aeross-in~~ the Northern Gulf of Alaska with differing oceanographic conditions and farming practices to determine the carbon sequestration potential over the growing season. Sensors were deployed on two subsurface moorings placed in proximity of one another at each farm site: one “inside” and one “outside” as a ~~control-reference~~ upstream of the farm. Both sensor arrays conducted hourly measurements of pH or CO₂, temperature, salinity, and oxygen during the time from seed line outplanting in winter (November to January) to spring harvest (April or May) in 2024. Nominal differences in carbonate chemistry parameters were detected between the inside and outside moorings until March, when the frequency of variability remained consistent between moorings but their respective magnitude diverged. Notably, apparent oxygen production, seawater CO₂ concentration, air-sea CO₂ flux, and ~~the~~ strength of periodic signals varied by farm site. Integrated over the entire deployment, ~~two-one~~ farms demonstrated net negative air-sea CO₂ fluxes while one served as a net source of carbon over the deployment period: $-84,397 \pm 41,374 \text{ mol m}^{-2}$ in Jakolof Bay, $-11,115 \pm 1,331,480.3 \pm 87.5 \text{ mol m}^{-2}$ in Kalsin Bay, and $-9,23543 \pm 3.621 \text{ mol m}^{-2}$ in Windy Bay. This study highlights the nuance of farmed kelp carbon capture by demonstrating that farm site can influence overall air-sea CO₂ flux and that kelp farms are not always a net sink for atmospheric carbon.

1 Introduction

Since the Industrial Revolution, the global ocean has absorbed almost one-third of anthropogenically produced CO₂ (Feely et al. 2004; Quéré et al. 2018), driving a process termed ocean acidification. OA has direct and indirect deleterious effects on marine organisms such as shell dissolution in crustaceans and mollusks (Ries et al. 2016), malfunctioning olfactory responses in salmon (Williams et al. 2019), and stunted growth and development across trophic levels (Kurihara et al. 2013; Bignami et al. 2013; Long et al. 2013; Alcantar et al. 2024). If elevated CO₂ emissions to the atmosphere are not reduced, the poorest and most vulnerable human populations are most likely to suffer losses and damages as a result (IPCC 2022). To help curtail the impacts of these climactic changes, efforts to sequester carbon in ocean environments have been proposed and referred to as

Formatted: Superscript

Formatted: Superscript

marine carbon dioxide removal (mCDR). mCDR methods aim to enhance the flux of CO₂ into the ocean through techniques such as ocean fertilization, ocean alkalization enhancement, artificial upwelling, and kelp carbon sequestration (DeAngelo et al. 2023; Oeschlies et al. 2025).

The burial of biomass from highly productive organisms, such as seaweed, has shown promise as a sustainable option for capturing carbon through enhanced photosynthesis (Jiang et al. 2013; Ikawa and Oechel 2015). ~~A recent study characterized the average rate of organic carbon burial in sediments at 20 seaweed farms at $2.41 \pm 1.68 \text{ mmol C m}^{-2} \text{ yr}^{-1}$, placing seaweed farms on the low end of burial rates in natural marine carbon sinks (Duarte et al. 2025).~~ While the nearshore environment generally acts as a source of CO₂ to the atmosphere due to net heterotrophy (Chen and Borges 2009; Cai 2011), many kelp farms around the world have demonstrated that atmospheric CO₂ can be taken up by kelp and converted into seaweed biomass (Ikawa and Oechel 2015; Jiang et al. 2015; Mongin et al. 2016). ~~For the ocean to effectively absorb atmospheric CO₂, atmospheric CO₂ levels must be in disequilibrium with the ocean, which is dependent on factors such as wind and temperature (Wanninkhof 2014).~~ In Lidao town, China, a kelp farm exhibited variation in net autotrophic activity throughout the year with the greatest drawdown of atmospheric CO₂ in spring and the least amount in summer (Jiang et al. 2013). However, to achieve climate benefits, kelp farming would need to expand significantly, covering over 90,000 km² (Coleman et al. 2022; DeAngelo et al. 2023). ~~Furthermore, seaweed would need to absorb an estimated 4 Gt CO₂ yr⁻¹ to achieve net zero emissions by 2050, though considerable uncertainty remains around these estimations (Arzeno-Soltero et al. 2023).~~ Given the scale of such efforts, other, more logistically feasible approaches have been proposed, such as implementing the use of kelp farms to locally reduce atmospheric CO₂ concentrations by shifting the magnitude and timing of carbon cycling. There are negative effects to consider when increasing the footprint of kelp farms as well, such as the reduction of marine recreational access, hazards to navigation, and the removal of nutrients when the kelp biomass is removed from the water (National Academy of Sciences, Engineering, and Medicine 2021).

The Northern Gulf of Alaska (NGA) has been identified as a potential site for scaling up kelp farming due to its vast coastline, highly productive waters, and the need to help transition the state economy away from heavy reliance on fossil fuel extraction and unpredictable wild fish stocks (Miller 2021; Bullen et al. 2024; Edgar et al. 2024). As a result, the NGA kelp farming industry expects to expand dramatically in the next two decades, increasing sustainable economic practices in the state with the added benefit of enabling the Alaskan coastal system and adjoining federal waters to potentially take up excess atmospheric CO₂. Empirical rate estimates of CO₂ drawdown by kelp from other regions are not universally applicable, due to the site-specific interaction of many physical and biological factors that affect kelp-related CO₂ flux rates (Ikawa and Oechel 2015; Jiang et al. 2015; Mongin et al. 2016). Accordingly, Alaska-specific values are needed, so that we may better assess the climate benefits of kelp farming in the NGA.

In the NGA, seeded lines are deployed between October and January, and harvested in late spring before biofouling by epiphytic organisms (Stekoll et al. 2021). Coastal marine ecosystems in the NGA are generally net heterotrophic, aside from approximately sixty days ~~sixty days~~ of net autotrophy in summer and early fall (Miller and Kelley 2021); however, offshore

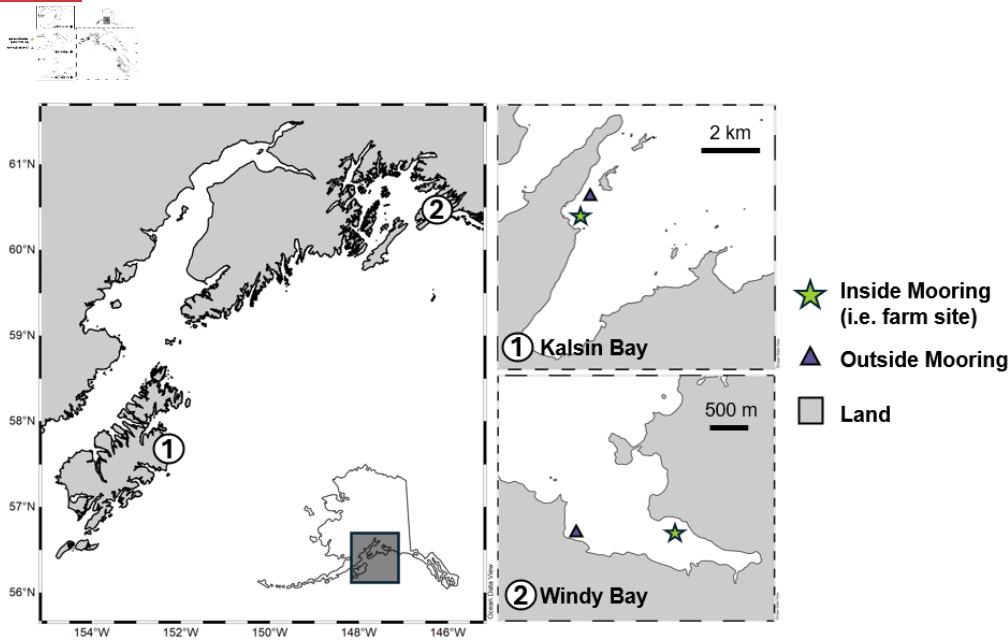
on the continental shelf, the ocean acts primarily as a carbon sink (Evans and Mathis 2013). Currently, there are no estimates
65 of kelp farm air-sea CO₂ fluxes in the NGA, although nearshore macroalgal-dominated habitats can alter carbonate chemistry
and create seasonal, localized carbon sinks, signaling the potential to utilize farmed seaweed as one mechanism to reduce
atmospheric CO₂ concentrations (Miller and Kelley 2021). This study quantified the air-sea CO₂ flux in ~~three-two~~ kelp farms
~~aeross-in~~ the NGA to determine the capacity of farmed kelp to take-up CO₂ relative to adjacent waters. This study provides
empirical estimates of kelp farm-related CO₂ flux, thus identifying the role that Alaska's kelp farming industry can play in
70 reducing atmospheric CO₂ and highlighting the capacity of farms to offset anthropogenic CO₂ emissions.

2 Materials and methods

2.1 Site descriptions

~~Three-Two~~ nearshore kelp farms were selected ~~aeross-from~~ the Northern Gulf of Alaska (NGA) spanning a distance of ~~_over~~
400 km: ~~Spinnaker Sea Farms in Jakolof Bay (59.4604 °N, 151.5193 °W)~~, Royal Ocean Kelp Co in Windy Bay (60.5628 °N,
75 145.9569 °W), and Alaska Ocean Farms in Kalsin Bay (57.6581 °N, 152.4201 °W) (Fig. 1). The ~~three-two~~ farm sites varied
in size, harvest period, and species grown. ~~Spinnaker Sea Farms in Jakolof Bay covered 7,500 m² and grew *Saccharina*~~
~~*latissima* and *Alaria marginata*. The farm also cultivated Pacific oysters (*Crassostrea gigas*) in lantern nets and metal cages~~
~~on a longline on the inner side of the farm. Seed lines (i.e., lines populated with young sporophytes) were outplanted in~~
~~December and harvested in late April. The average water column depth at the farm shifted from 5.5 m to 10 m depending on~~
80 ~~the tide. Due to elevated light availability associated with the shallow water column across the entirety of Jakolof Bay, the~~
~~muddy to rocky benthos is covered with wild *S. latissima*.~~ Alaska Ocean Farms in Kalsin Bay, in operation for three years,
covered 3,200 m² and grew only *A. marginata*. Seed lines were outplanted in January and harvested in late May. The depth of
the site varied from 9 to 18 m with a tidal range of up to 3 m. The substrate was largely composed of sand. Royal Ocean Kelp
Co in Windy Bay covered 12,000 m² and contained two catenary arrays: one of *S. latissima* and one of *A. marginata* suspended
85 at approximately 2.2 m and 1.2 m depth, respectively. The eight lines making up each array were spaced 3 m apart. Seed lines

were outplanted in October and harvested in early May. The water column depth at the farm varied from 12 m to 22 m with a tidal range of 5.5 m. The substrate was largely made up of mud. ~~None~~ Neither of these sites are glacier-influenced.



90 **Figure 1:** Map of the two kelp farm study sites: Spinnaker Sea Farms in Jakolof Bay, Alaska Ocean Farms in Kalsin Bay, and Royal Ocean Kelp Co. in Windy Bay. An “inside mooring” was deployed within the farm and an “outside mooring” was deployed upstream of the farm to act as a reference control for background respiration and photosynthesis. The distance between these moorings was 50 m in Jakolof Bay, 100 m in Kalsin Bay, and 600 m in Windy Bay. All arrays suspended 3 m below the surface, roughly the depth of the growing kelp.

95 2.2 Sensor deployments, calibrations, and carbonate system calculations

A sensor array was deployed inside and outside of each farm (Fig. 1). To accurately estimate net air-sea CO₂ flux of kelp farms through time, the outside mooring must be influenced by the same water mass as the farm to capture background photosynthesis and respiration. In general, the “inside” sensor array was positioned as close to the center of the farm as possible and supported by a buoy. The “outside” sensor array was placed on a mooring a distance from the farm to ensure that it was not influenced by the biological activity of the farm while still experiencing the same water masses (Fig. 1). Given the different bathymetric and hydrologic features at each farm site, placement distance between the arrays varied; however, the depth of both the inside and outside mooring within the water column were similar across sites. Each sensor array was outfitted with a minimum of a

100

105 Sea-Bird SeapHOxTM (combination of the SeaFETTM pH sensor and the SBE 37-SMP-ODO MicroCAT CTD+DO sensor) or a Sunburst SAMI-CO₂TM, a PME miniDOT optical oxygen logger, and an Onset HOBO conductivity logger, a Sea-Bird SeapHOxTM (combination of the SeaFETTM pH sensor and the SBE 37-SMP-ODO MicroCAT CTD+DO sensor) in Windy Bay, and a Sunburst SAMI-CO₂TM in Kalsin Bay. The sensor arrays were suspended roughly 3 m from the surface, which is the same depth as the growing kelp which may misrepresent the flux in highly stratified settings. However, NGA bays experience well-mixed water columns due to the strong tidal mixing (Haag et al. 2023), indicating that in locations without strong freshwater input a sensor placed at 3 m depth would be representative of the near surface. All parameters were measured on a frequency of one hour.

110 Calibration and reference seawater bottle samples were collected by farmers when they visited their farms by lowering a Science FirstTM 1.5L Water Sampler to the depth of the sensor array and filling 250 mL borosilicate bottles pre-spiked with 200 μ l saturated mercuric chloride. During the retrieval of the sensors at each site in spring/summer, a survey was conducted to capture within-farm spatial variability in carbonate chemistry by collecting water samples in a grid formation at the depth of the kelp using the same methods as above. The discrete bottle samples were analyzed for pH_T (total scale) if complementing the pH sensors or dissolved inorganic carbon (DIC) if complimenting the CO₂ sensors, and all samples were analyzed for total alkalinity (TA) and salinity. A Shimadzu 1800 spectrophotometer was used to measure seawater pH_T using meta-cresol purple as an indicator dye (Acros, batch #30AXM-QN), and applying a dye impurity correction factor (Douglas and Byrne 2017). A DIC Analyzer (Apollo SciTech, Model AS-C6L) coupled to a LI-7815 CO₂/H₂O Analyzer measured DIC using a three-point calibration of Certified Reference Material (CRM: Batch 172, A.G. Dickson, Scripps Institute of Oceanography). A Metrohm 848 Titrino plus measured TA via an open-cell titration and a YSI 3100 Conductivity instrument measured salinity.

125 The SeaFETs were calibrated using the pH_T measured from the discrete seawater samples by calculating electrode specific single-point calibration coefficients, which were then used to derive the entire pH dataset (Bresnahan et al. 2014; Miller et al. 2018). The HOBO loggers were calibrated with the HOBOWare[®] Pro software using the salinity and temperature measured by either the CTD within the SeapHOx or with the discrete bottle samples. The SAMI-CO₂ timeseries was translated up or down relative to the discrete water samples. The miniDOTs were calibrated using the mean atmospheric pressure and salinity over the deployment. Data can be accessed from the DataONE repository (<https://doi.org/10.24431/rw1k9hb>).

130 Calculations were conducted in R (version 4.4.1) and MATLAB (version R2024b). The uncertainty associated with the pH_T timeseries was calculated following Bresnahan et al. (2024) and Miller and Kelley (2021). In short, the propagated uncertainty incorporated all sources of possible error in the sample analysis procedure: the difference in the lab measurement of pH_T and TA on a known CRM bottle versus the expected values, the standard deviation of the duplicate calibration bottle measurements, and the constants error for the CO₂ conversions (version 2.3; Lewis and Wallace 1998). Total uncertainty was calculated by adding the propagated uncertainty to the difference between a reference bottle and the calibrated pH timeseries (following Miller and Kelley 2021). The pH uncertainty was then converted to an in situ partial pressure of CO₂ (pCO₂) uncertainty using a Monte Carlo simulation whereby the pH uncertainty was used to create a series of perturbed pH values for each timepoint (n

= 10,000) that were then converted to $p\text{CO}_2$ using the 'seacarb' package in R (version 3.3.3; Gattuso et al. 2015). When summarizing the timeseries data and spatial survey to single means, the standard deviation was reported to capture the natural variability of the value and not the total uncertainty.

The 'seacarb' package can estimate any carbonate system parameters using two known values. The calibrated pH timeseries was used in ~~Jakolof Bay and~~ Windy Bay as the first variable and TA was the second variable calculated from salinity using a known salinity-TA relationship for the nearshore of the NGA (Evans et al. 2015; see Fig. A1), while $p\text{CO}_2$ was ~~used directly measured in Kalsin Bay for air-sea flux estimates. However, the decomposition analysis required a TA estimation for Kalsin Bay and the Evans et al. (2015) relationship is not a good proxy for this location based on a sensitivity analysis adapted from Fassbender et al. (2017) (see Appendix). A site-specific salinity-TA equation was estimated using a linear model for this purpose (Fig. A1)~~The second variable across all sites was TA calculated from salinity using a known salinity-TA relationship for the nearshore of the NGA (Evans et al. 2015; see Fig. A1). The $p\text{CO}_2$ timeseries ~~was were~~ subsequently used to calculate air-sea CO_2 fluxes (FCO_2) following Eq. 1 by Wanninkhof (2014):

$$\text{FCO}_2 = 0.251U^2(\text{Sc}/660)^{-0.5}K_0(p\text{CO}_{2w} - p\text{CO}_{2a}), \quad (1)$$

where U is the wind speed in m s^{-1} , $\text{Sc}/660$ is the dimensionless Schmidt number, K_0 is the Bunsen solubility coefficient with units of $\text{mol L}^{-1} \text{atm}^{-1}$, and $p\text{CO}_{2w}$ and $p\text{CO}_{2a}$ are the $p\text{CO}_2$ in water and air, respectively. Site-specific wind data was obtained from the nearest NDCB buoy to the farm site: Station CRVA2 for Windy Bay located 7 km from the farm and Station KDAA2 for Kalsin Bay located 8 km from the farm (NOAA Buoy Data Center (2024)). ~~The near-surface winds at the farm may differ from the wind speed detected at the buoys, therefore giving first-order estimates of the exchange rates rather than precise local fluxes.~~ $p\text{CO}_{2a}$ was assumed to be ~ 421.2 ppm at all sites (McKain et al. 2024). $\text{Sc}/600$ and K_0 were calculated using the polynomial equations in Wanninkhof (2014). In the absence of wind, the above equation becomes simplified as per MacIntyre (1995) to:

$$\text{FCO}_2 = 0.8K_0(p\text{CO}_{2w} - p\text{CO}_{2a}), \quad (2)$$

since atmospheric exchange continues even when turbulent mixing at the water surface does not occur. The net FCO_2 , a measure of the kelp farm effect, was calculated by subtracting the FCO_2 estimated for the inside mooring from the outside mooring for each farm site location and integrating over the entire timeseries. An uncertainty for total net integrated FCO_2 was calculated by propagating the errors associated with each of the sensors and the data pulled from online resources through the air-sea flux calculation and integration.

2.2 Ancillary data analysis

Temperature-salinity (T-S) diagrams were used to determine if the inside and outside moorings experienced the same water mass, since a water mass can be defined by their salinity and potential temperature as those variables remain conserved unless experiencing mixing conditions. T-S diagrams were created by modifying the 'ggTS' function (Kaiser 2020), which utilized

Formatted: Not Highlight

the ‘gsw’ package to calculate the potential density and plot isopycnals (version 1.2-0; Kelley et al. 2024). Similarities between the T-S diagrams for both moorings would indicate that the outside mooring can act as a ~~control-reference~~ for the inside mooring. The lag time ~~of the water mass~~ between the outside and inside moorings were characterized by detrending the data and applying a cross-correlation using the ‘tseries’ package (version 0.10-58; Trapletti et al. 2015).

The timeseries at each site was divided into three phases in order to compare carbonate chemistry shifts throughout the kelp growing season: heterotrophy, transitional, and autotrophy. Net heterotrophy or autotrophy of seawater was determined by calculating the apparent oxygen production (AOP) across the timeseries, which is the difference between the measured *in-situ* oxygen versus the estimated oxygen saturation as a function of temperature and salinity (Garcia and Gordon 1992: equations corrected from Casamitjana and Roget 1993). The shift from heterotrophy or autotrophy to the transitional phase was characterized as the first twenty-four-hour period in which average daily AOP shifted from positive to negative or vice versa, and the shift from the transitional phase back to either heterotrophy or autotrophy was characterized as a period of time when daily averaged AOP remained either positive or negative for over one week.

The drivers of seawater $p\text{CO}_2$ were assessed by doing a decomposition of monthly averages of $p\text{CO}_2$ based on the effects of temperature (T), salinity (S), total alkalinity (TA), air-sea CO_2 flux (FCO_2), and dissolved inorganic carbon (DIC). The following equations were modified from Garcia-Troche et al. (2021), originally based on pH, to describe observed monthly changes between two consecutive months (t_1 and t_2):

$$\Delta p\text{CO}_2 = \Delta p\text{CO}_2(T) + \Delta p\text{CO}_2(S) + \Delta p\text{CO}_2(TA) + \Delta p\text{CO}_2(\text{FCO}_2) + \Delta p\text{CO}_2(\text{DIC}) + R, \quad (3)$$

where a change in seawater $p\text{CO}_2$ from one month to another ($\Delta p\text{CO}_2$) can be described as the changes to the five variables plus a residual (R), which represents any remaining $\Delta p\text{CO}_2$ not explained by T, S, TA, FCO_2 , or DIC. Using the ‘seacarb’ package in R, the stepwise calculated change in $p\text{CO}_2$ between t_1 and t_2 was derived by a single variable at a time to calculate the monthly $\Delta p\text{CO}_2(T)$, $\Delta p\text{CO}_2(S)$, and $\Delta p\text{CO}_2(TA)$:

$$\Delta p\text{CO}_2(T) = \Delta p\text{CO}_{2,2}(T_2, S_1, TA_1, \text{DIC}_1) - \Delta p\text{CO}_{2,1}, \quad (4)$$

$$\Delta p\text{CO}_2(S) = \Delta p\text{CO}_{2,2}(T_1, S_2, TA_1, \text{DIC}_1) - \Delta p\text{CO}_{2,1}, \quad (5)$$

$$\Delta p\text{CO}_2(TA) = \Delta p\text{CO}_{2,2}(T_1, S_1, TA_3, \text{DIC}_1) - \Delta p\text{CO}_{2,1}, \quad (6)$$

Due to DIC exerting an effect on both $\Delta p\text{CO}_2(\text{FCO}_2)$ and $\Delta p\text{CO}_2(\text{DIC})$, as a result of air-sea CO_2 exchange and water column/benthic processes, respectively, $\Delta p\text{CO}_2(\text{FCO}_2)$ was calculated first and subsequently used to separate its signal from $\Delta p\text{CO}_2(\text{DIC})$. $\Delta p\text{CO}_2(\text{FCO}_2)$ required an estimate of monthly CO_2 air-sea exchange calculated using Eq. 1 and 2 (i.e., FCO_2), the change in time ($t_2 - t_1$, days), seawater density (d , kg m^{-3}), and ~~sampled-water column height depth~~ (H, m) from Garcia-Troche et al. (2021):

$$\Delta \text{DIC}_{\text{air-sea}} = \frac{-\text{FCO}_2 \times (t_1 - t_2)}{d \times H}, \quad (7)$$

$$\Delta pCO_2(FCO_2) = \Delta pCO_{2,2}(T_1, S_1, TA_1, DIC_1 + \Delta DIC_{air-sea,2}) - \Delta pCO_{2,1}, \quad (8)$$

$$\Delta pCO_2(DIC) = \Delta pCO_{2,2}(T_1, S_1, TA_1, DIC_2) - \Delta pCO_2(FCO_2) - \Delta pCO_{2,1}, \quad (9)$$

The monthly periodicity of pCO_2 was estimated with a power spectral analysis using R package ‘spectrum’ (version 1.1; John and Watson 2020). The span was set to 20 days. A high-pass Butterworth filter (package ‘signal’; version 1.8-1; Ligges et al. 2015) was first applied to remove low-frequency components that can dominate the spectrum. The cutoff was set to 0.01 cycles per hour. The underlying periodicities were plotted to visually determine the dominant drivers of pH_T frequency.

3 Results

3.1 Comparison of inside and outside moorings

Comparison of water mass movement at the inside and outside moorings confirmed that both sensor arrays detected similar water masses, allowing for a calculation of net air-sea CO_2 flux when paired with the inside sensor array. T-S diagrams were remarkably similar between inside and outside moorings across all sites, with distinct shifts through time driven by temperature, denoted in the color overlay (Fig. 2). Salinity remained relatively consistent through the deployment period (~~30.9 ± 0.4 in Jakolef Bay,~~ 30.0 ± 0.6 in Kalsin Bay; and 31.1 ± 0.4 in Windy Bay) while temperature at ~~all three both~~ sites decreased from winter to early spring before warming once again (Fig. 2). The inflection of temperature warming occurred at different times depending on the site: ~~early March in Jakolef Bay,~~ mid-March in Kalsin Bay; and mid-April in Windy Bay. The cross-correlations measured between salinity and temperature at the paired moorings indicate a lag time of ~~0 hours in Jakolef Bay,~~ 1 hour according to salinity and 0 hours according to temperature in Kalsin Bay, and 1 hour in Windy Bay for both variables, demonstrating strong similarities at the inside and outside moorings.

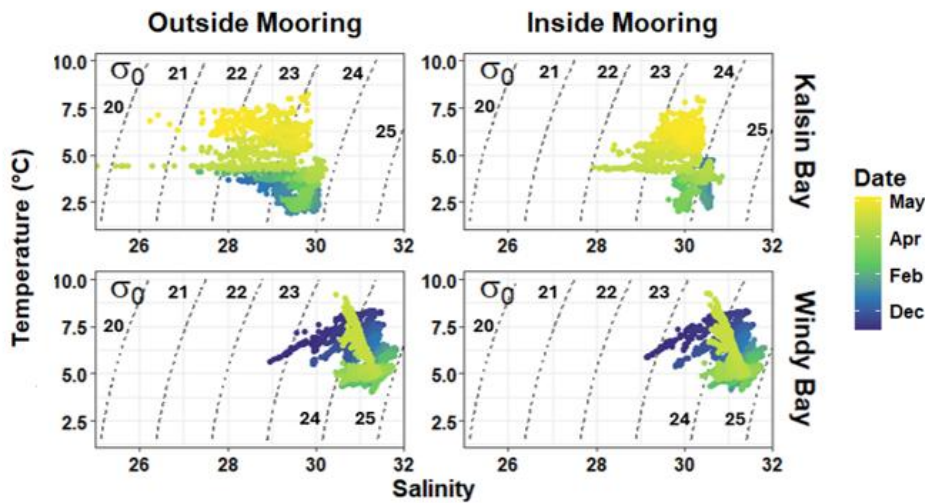
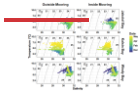


Figure 2: Temperature-salinity diagrams from ~~three-two~~ locations in the Northern Gulf of Alaska at moorings within kelp farms (inside moorings) and ~~control-reference~~ moorings upstream of the farm sites (outside moorings). Sensor arrays collected hourly data from 3 m depth. Labelled dashed lines denote isolines of potential density (σ_θ ; -1000 kg m^{-3}).

Apparent oxygen production (AOP), the difference between *in situ* O_2 and O_2 saturation estimated as a function of temperature and salinity, demonstrated that ~~the-both~~ nearshore systems ~~at-each-site~~ experienced a distinct shift from net heterotrophy to net autotrophy throughout the growing season (Fig. 3). ~~All-Both~~ sites began with net heterotrophy in winter and, as spring progressed, neared the solubility compensation point (AOP = 0) where the system shifted to a transitional phase (~~on-April-2-in~~ ~~Jakolof-Bay~~, February 13 in Kalsin Bay, and March 20 in Windy Bay). The length of this transitional phase varied depending on location: ~~23-days-in-Jakolof-Bay~~, 0 days in Kalsin Bay, and 13 days in Windy Bay. Kalsin Bay and Windy Bay became net autotrophic during the kelp growing season on February 13 and April 2, respectively, ~~while-Jakolof-Bay-remained-near-the-solubility-compensation-point-until-after-kelp-harvest~~ (Fig. 3). ~~The-inside-mooring-demonstrated-greater-net-heterotrophy-than-the-outside-mooring-in-Jakolof-Bay-starting-in-late-March~~. ~~In-Windy-Bay-and-Kalsin-Bay~~, ~~At-both-sites~~, the inside mooring was characterized by higher net autotrophy than the outside mooring as time neared harvest (Fig. 3).

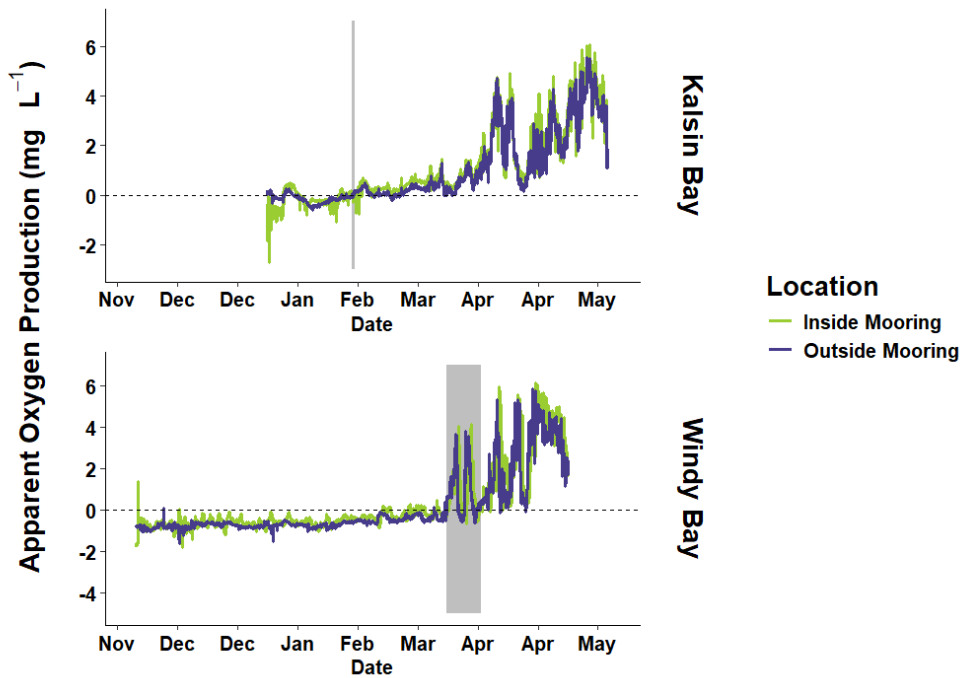


Figure 3: Apparent oxygen production (i.e. measured O_2 minus saturated O_2) across the farmed kelp growing season and the following summer in **Jakolof Bay**, Kalsin Bay, and Windy Bay both inside the farm (inside mooring) and at the **control-reference** site outside of the farm (outside mooring). The dashed line indicates when measured O_2 is equal saturated O_2 and thus denotes the solubility compensation point. The grey boxes indicate the transitional period from net heterotrophy to net autotrophy in spring.

During the net heterotrophic wintertime phase described by AOP, **all three both** timeseries displayed ambient seawater (i.e. the outside mooring) pCO_2 values greater than atmospheric CO_2 (i.e. $421.2 \mu atm$; McKain et al. 2024; Fig. 4). In Windy Bay, the inside and outside moorings had associated total uncertainties of $69.46 \mu atm$ and $73.73 \mu atm$, respectively, **and in Jakolof Bay,** **the inside and outside moorings had associated total uncertainties of $93.45 \mu atm$ and $91.06 \mu atm$, respectively.** The average pCO_2 at the outside mooring during this net heterotrophic period **was $454.1 \pm 15.0 \mu atm$ in Kalsin Bay ($n = 772$) and was $448.2 \pm 21.9 \mu atm$ for Jakolof Bay ($n = 2812$), and $482.2 \pm 22.4 \mu atm$ for in Windy Bay ($n = 2854$).** **Note that the pCO_2 data in Kalsin Bay began during the autotrophic period (Fig. 4).** From the beginning of the transitional period to kelp harvest,

seawater $p\text{CO}_2$ decreased below atmospheric CO_2 at two of the three both sites, Kalsin Bay and Windy Bay, with a concurrent increase in $p\text{CO}_2$ variability (Fig. 4). The total average $p\text{CO}_2$ at the outside mooring during this time was $326.817.5 \pm 94.291.3$ μatm for Kalsin Bay ($n = 21332341$) and 306.1 ± 99.3 μatm for Windy Bay ($n = 1145$). In contrast, in Jakolof Bay the total average $p\text{CO}_2$ at the outside mooring was 604.2 ± 370.1 μatm ($n = 522$) with a maximum of 2958.4 μatm in late April. It must be noted that the moorings in Jakolof Bay were heavily colonized by wild kelp, whereas biofouling at the other two sites was minimal (see Fig. A2).

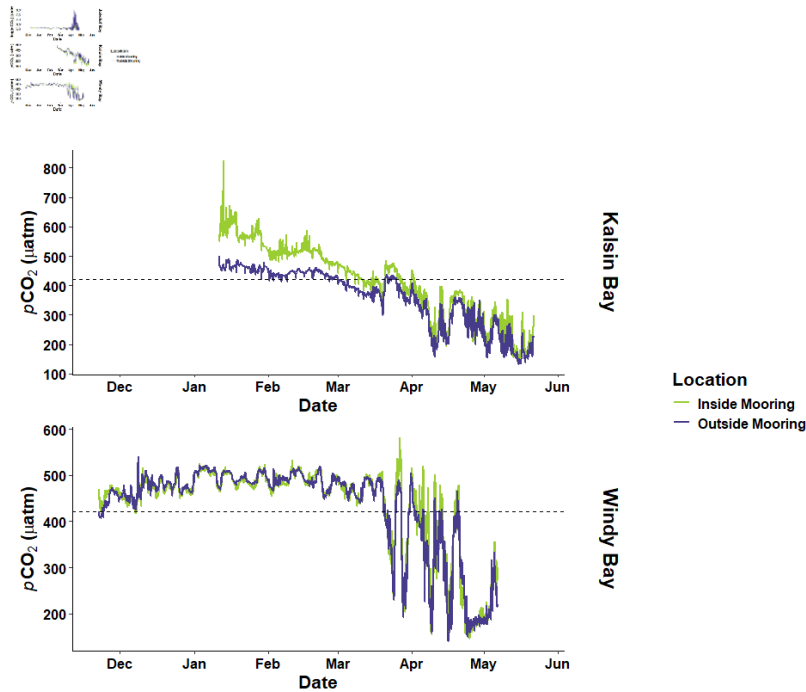


Figure 4: The partial pressure of carbon dioxide ($p\text{CO}_2$) in seawater inside and outside of kelp farms across the kelp growing season in Jakolof Bay (note the log axis), Kalsin Bay, and Windy Bay. The dashed line indicates the atmospheric CO_2 value which has been estimated to be ~ 421.2 ppm at all sites (McKain et al. 2024).

The variability in $p\text{CO}_2$ was consistent between the inside and outside moorings throughout the entire deployment period, although after shifting from heterotrophy to autotrophy, the magnitude of variability increased at the inside mooring, clearly indicating the influence of kelp biological processing (Fig. 4). During the wintertime net heterotrophic phase, the absolute difference in $p\text{CO}_2$ at the inside versus outside moorings differed an average of 102.3 ± 38.1 μatm in Kalsin Bay ($n = 772$)

260 ~~and $10.1 \pm 10.0 \mu\text{atm}$ in Jakolof Bay ($n = 2812$) and $7.2 \pm 6.5 \mu\text{atm}$ in Windy Bay ($n = 2854$). From the beginning of the transitional period to kelp harvest, the absolute difference in seawater $p\text{CO}_2$ at the inside mooring versus the outside mooring ranged between 0.1 to $2500.3 \mu\text{atm}$ in Jakolof Bay ($186.0 \pm 312.3 \mu\text{atm}$, $n = 522$), between -0.0002 to $140.7272 \mu\text{atm}$ in Kalsin Bay (38.4352 ± 21.1484 , $n = 2341333$), and 0.01 to $147.1 \mu\text{atm}$ in Windy Bay ($26.3 \pm 23.2 \mu\text{atm}$, $n = 1145$). $p\text{CO}_2$ was lower-higher at the inside mooring than the outside mooring during this later part of the deployments in in Jakolof Bay and Kalsin Bay and, whereas values at the inside mooring exceeded those of the outside mooring in Windy Bay (Fig. 4). In short, the differences in $p\text{CO}_2$ between the moorings increased as the kelp growing season progressed.~~

3.2 Air-sea CO_2 flux timeseries

270 Air-sea CO_2 flux estimations (FCO_2) for all sites and moorings demonstrated a flux of CO_2 from the ocean to the atmosphere during the net heterotrophic period indicated by AOP (Fig. 3; Fig. 5). The FCO_2 for the outside mooring during this period ranged between -0.015 to $0.599 \text{ mmol m}^{-2} \text{ h}^{-1}$ in Kalsin Bay ($0.047 \pm 0.077 \text{ mmol m}^{-2} \text{ h}^{-1}$, $n = 772$) and -60.3 to $204.0 \text{ mmol m}^{-2} \text{ d}^{-1}$ in Jakolof Bay ($6.7 \pm 12.3 \text{ mmol m}^{-2} \text{ d}^{-1}$, $n = 2812$) and -0.069 to $1.253 \text{ mmol m}^{-2} \text{ h}^{-1}$ in Windy Bay ($0.05656 \pm 0.1111 \text{ mmol m}^{-2} \text{ h}^{-1}$, $n = 2854$). As the period of net heterotrophy ended, Kalsin Bay and Windy Bay both sites became carbon sinks while Jakolof Bay remained as a source of carbon to the atmosphere. The proportional difference in FCO_2 between moorings (i.e., the FCO_2 at the inside mooring divided by the outside mooring) increased at all both sites over time (see Fig. A23), demonstrating that as the kelp growing season progressed, so did the difference in FCO_2 estimated at the paired moorings.

275 FCO_2 at the outside mooring ranged between -61.2 to $2453.5 \text{ mmol m}^{-2} \text{ d}^{-1}$ in Jakolof Bay ($43.2 \pm 191.3 \text{ mmol m}^{-2} \text{ d}^{-1}$, $n = 652$), -1.624785 to $0.22732 \text{ mmol m}^{-2} \text{ h}^{-1}$ in Kalsin Bay ($-0.084115 \pm 0.178187 \text{ mmol m}^{-2} \text{ d}^{-1}$, $n = 2341335$), and -1.016 to $0.456 \text{ mmol m}^{-2} \text{ h}^{-1}$ in Windy Bay ($-0.047 \pm 0.117 \text{ mmol m}^{-2} \text{ h}^{-1}$, $n = 2492$). The astronomical rise in FCO_2 in April at the outside mooring in Jakolof Bay was mirrored at the inside mooring (Fig. 5), though the maximum FCO_2 inside the farm was $222.0 \text{ mmol m}^{-2} \text{ d}^{-1}$, an order magnitude smaller than the largest flux outside the farm. The similarities in the trend at both moorings in Jakolof Bay lend confidence that the ambient water at this site continued to be a source of carbon to the atmosphere in early spring.

Formatted: Not Highlight

Formatted: Not Highlight

Formatted: Not Highlight

Formatted: Not Highlight

Formatted: Not Highlight

Formatted: Not Highlight

Formatted: Not Highlight

Formatted: Not Highlight

Formatted: Not Highlight

Formatted: Not Highlight

Formatted: Not Highlight

Formatted: Subscript

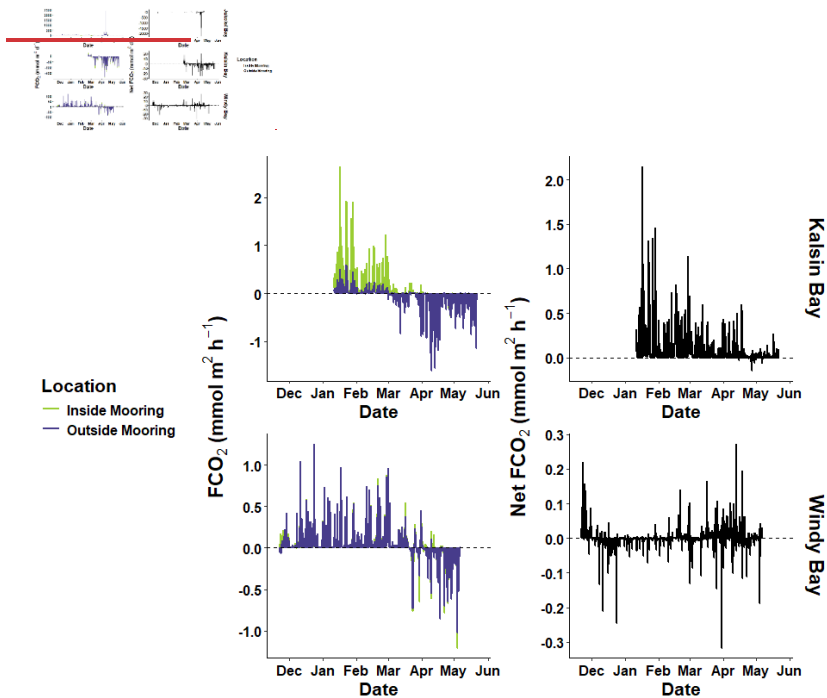


Figure 5: The partial Variation in air-sea CO₂ fluxes (FCO₂) across the kelp growing season at three different sites and the net FCO₂ representing the inside versus the outside fluxes.

The influence of the kelp farms created a carbon sink at Jakolof Bay and Kalsin, Windy Bay, but a carbon source at Windy Kalsin Bay (Fig. 5). Net FCO₂, the difference in FCO₂ at the inside versus outside moorings representing the farm signal, integrated from the start of the transitional period (Fig. 2) to harvest over the entire kelp growing season was -84,397 ± 41,374 mol m⁻² in Jakolof Bay, -11,115480.3 ± 1,33187.5 mol m⁻² in Kalsin Bay, and -9,2543 ± 03.624 mol m⁻² in Windy Bay. The small net positive integrated FCO₂ in Windy Bay was due to equal variation in FCO₂ above and below zero throughout the sensor deployment (Fig. 5). The net FCO₂ across the timeseries was within the same magnitude as those of the outside mooring, indicating that large differences were experienced at the inside and outside moorings of each both sites.

The inside mooring value corresponded with the spatial samples collected at Kalsin Bay at the time of kelp harvest, while the mooring underestimated the FCO₂ of the farm spatial sampling at Jakolof Bay and Windy Bay (Fig. 6). The spatial surveys at each farm indicated a FCO₂ of 4.1 ± 0.9 mmol m⁻² d⁻¹ at Jakolof Bay (n = 9), -0.150 ± 0.183 mmol m⁻² d⁻¹ at Kalsin Bay (n = 8), and 0.0494 ± 0.0077 mmol m⁻² d⁻¹ at Windy Bay (n = 9). The FCO₂ of the sample collected at the outside mooring

Formatted: Not Highlight

Formatted: Not Highlight

Formatted: Not Highlight

Formatted: Superscript

Formatted: Superscript

Formatted: Not Highlight

Formatted: Not Highlight

Formatted: Not Highlight

Formatted: Not Highlight

Formatted: Not Highlight

Formatted: Not Highlight

Formatted: Not Highlight

Formatted: Not Highlight

exceeded the farm samples in Jakolof Bay and in Windy Bay, but was lower at Kalsin Bay (Fig. 6). The FCO_2 estimate from the timeseries mooring in Kalsin Bay was within the spread of samples measured discretely at the farm, though one of the discrete bottle samples in the farm was comparable to the outside farm sample (Fig. 6). At In Jakolof Bay and Windy Bay, mooring values fell below the range measured discretely at the farm (Fig. 6). This spatial survey demonstrated the homogeneity of FCO_2 at the farm and discrepancy between the mooring timeseries and discrete bottle sample FCO_2 .

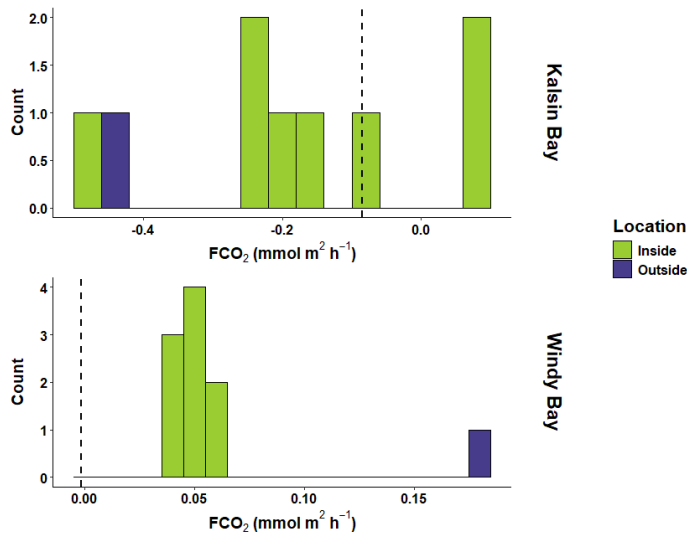


Figure 6: Scatterplot-Histogram denoting displaying the variation in air-sea CO_2 fluxes (FCO_2) across the kelp farm at three-two different sites directly right before harvest: April 23 in Jakolof Bay, May 22 in Kalsin Bay, ($n = 9$) and May 6 in Windy Bay ($n = 10$). The light bluegreen rectangles indicate the samples collected as a spatial survey within the farm, s the farm site and the samples taken within this location and the “outside” sample denoted in purple represents the ambient seawater of each bay at a mooring located upstream of the farm, and the dashed line represents the FCO_2 value estimated at the mooring inside the farm at the same timepoint.

3.3 Drivers of seawater $p\text{CO}_2$

The seawater $p\text{CO}_2$ decomposition demonstrated that monthly-hourly changes to $p\text{CO}_2$ were influenced primarily by biological processes and air-sea flux, as both $\Delta p\text{CO}_2(\text{DIC})$ and $\Delta p\text{CO}_2(\text{FCO}_2\text{TA})$ exerted the most considerable change in $p\text{CO}_2$ (Fig. 7). DIC and TA- FCO_2 applied both positive and negative changes to $p\text{CO}_2$ depending on site and time during the kelp growing season, but always as opposing forces. As temperature warmed throughout the spring, it decreased the capacity of $p\text{CO}_2$ to remain dissolved in seawater (Fig. 2; Fig. 7). Salinity and temperature played a negligible role in $\Delta p\text{CO}_2$ at all both sites during all months (Fig. 7). Therefore, the concentration of DIC and TA in seawater, controlled primarily by biological processes, had

Formatted: Subscript

Formatted: Subscript

Formatted: Subscript

the greatest influence on $\Delta p\text{CO}_2$, though the $\Delta p\text{CO}_2$ (DIC) term encompasses both water column and benthic processes and the hourly air-sea CO_2 flux drove the changes in seawater $p\text{CO}_2$. Therefore, it is not solely determined by the photosynthesis and respiration occurring in seawater but may also be influenced by benthic biogeochemical fluxes. The five drivers used to decompose the hourly changes in seawater $p\text{CO}_2$ included all major sources of variability in Kalsin Bay but not Windy Bay.

In Kalsin Bay, the remaining residuals ranged between $-3.6 \mu\text{atm}$ to $0.7 \mu\text{atm}$ ($-0.02 \pm 0.2 \mu\text{atm}$, $n = 3111$) at the inside mooring and $-12.3 \mu\text{atm}$ to $1.4 \mu\text{atm}$ ($-0.04 \pm 0.4 \mu\text{atm}$, $n = 3111$) at the outside mooring. In Windy Bay, the remaining residuals ranged between $-44.5 \mu\text{atm}$ to $2.4 \mu\text{atm}$ ($-0.3 \pm 1.6 \mu\text{atm}$, $n = 3997$) at the inside mooring and $-41.5 \mu\text{atm}$ to $0.7 \mu\text{atm}$ ($-0.3 \pm 1.5 \mu\text{atm}$, $n = 3997$) at the outside mooring. These residuals suggest that an additional moderate source of seawater $p\text{CO}_2$ was present in Windy Bay but not included as a parameter and was not captured in the decomposition analysis.

Formatted: Subscript

Formatted: Font: Italic

Formatted: Subscript

Formatted: English (Canada)

Formatted: English (United States)

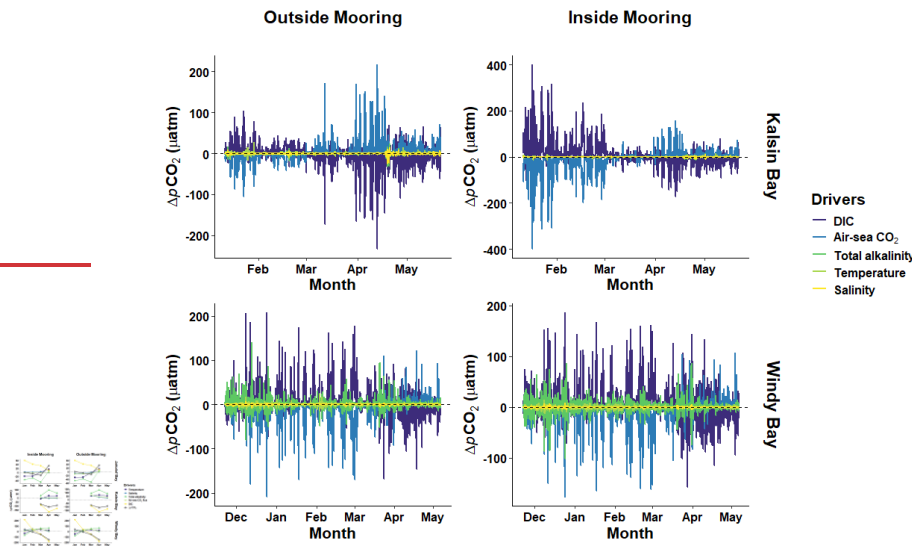
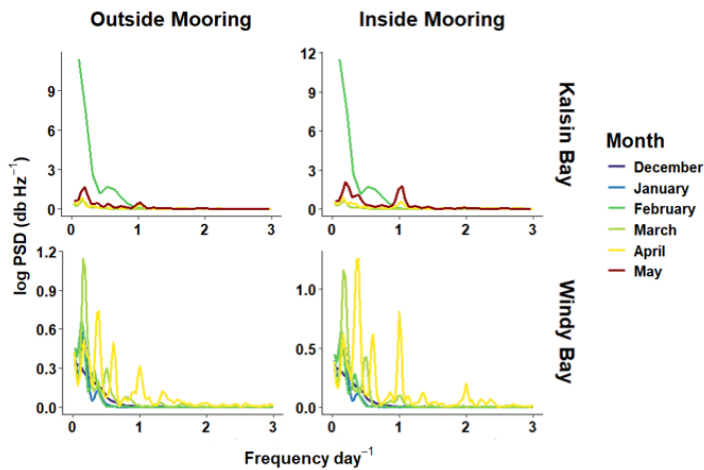


Figure 7: Cumulative monthly hourly changes in $p\text{CO}_2$ due to temperature, salinity, air-sea CO_2 flux, total alkalinity, and dissolved inorganic carbon. The analysis considered December as the starting point for Jakolof Bay and February as the starting point for Kalsin Bay and the prior month was used from thereon to calculate the change in $p\text{CO}_2$ in a given month.

The five drivers used to decompose the monthly changes in seawater $p\text{CO}_2$ did not include all sources of variability. There remained residuals of $-7.6 \mu\text{atm}$, $-4.4 \mu\text{atm}$, $-5.6 \mu\text{atm}$, and $0.4 \mu\text{atm}$ in Jakolof Bay (for January, February, March, and April, respectively), $-4.5 \mu\text{atm}$, $-57.3 \mu\text{atm}$, and $-38.8 \mu\text{atm}$ in Kalsin Bay (for March, April, and May, respectively), and -104.2

335 μatm , $-193.7 \mu\text{atm}$, $-191.0 \mu\text{atm}$, and $-65.9 \mu\text{atm}$ in Windy Bay (for January, February, March, and April, respectively). These residuals suggest that an additional sink of seawater $p\text{CO}_2$ was present but not included as a parameter, and was not captured in decomposition analysis.

The power spectral density (PSD) analysis revealed distinct site-specific and monthly differences in seawater $p\text{CO}_2$ periodicity that suggest diel and tidal cycling to be important drivers particularly as spring progresses (Fig. 8). Frequencies observed at 2 day^{-1} correspond to 12-hour cycles likely driven by tidal forcing. This frequency was strongly apparent in Jakolof Bay, to a lesser degree in Windy Bay, but not at Kalsin Bay (Fig. 8), suggesting that tides play a larger role in $p\text{CO}_2$ variability in Jakolof Bay than either Kalsin Bay or in Windy Bay but not Kalsin Bay. Frequencies corresponding to 1 day^{-1} , observed at all sites, also indicate a diel periodicity. The most likely driver of a diel cycle would be irradiance. Although temperature and salinity may change as a product of the day/night cycle, the decomposition of $p\text{CO}_2$ indicated that these factors played minimal roles in controlling seawater $p\text{CO}_2$ (Fig. 7). The outside mooring in Jakolof Bay demonstrated greater PSD at the tidal periodicity than the diel periodicity, while the opposite was true at the inside mooring, indicating that inside the farm the influence of photosynthesis during the day and respiration at night was stronger than what was observed for ambient seawater. There were multiple peaks $< 1 \text{ day}^{-1}$: 0.3 and 0.7 in Jakolof Bay, 0.3 in Kalsin Bay, and 0.3 and 0.6 in Windy Bay. Frequencies at 0.3, and 0.6, and 0.7 day^{-1} correspond to periodicity in seawater $p\text{CO}_2$ every 3.3 and 1.6, and 1.4 days. Further, the peaks of PSD grew stronger as the spring progressed with observable peaks beginning in April for Jakolof Bay and Kalsin Bay, and in March for Windy Bay (Fig. 8).



350 Figure 8: Monthly power spectral density analysis for Jakolof Bay, Kalsin Bay, and Windy Bay, inside and outside of the kelp farm at 3 m depth.

4 Discussion

355 ~~Three-Two~~ kelp farms ~~aeross-in~~ the Northern Gulf of Alaska (NGA) varied in the magnitude and direction of their influence on nearshore biogeochemistry. This study directly measured the effect of farmed kelp on the seawater carbonate system using four ~~or -to~~ six-month long sensor deployments recording hourly. Across the kelp growing season, which extends from winter to spring, ~~two-one~~ of the ~~two three~~ farms demonstrated a net negative integrated air-sea CO₂ flux (i.e., carbon moved from the atmosphere to the ocean) (Fig. 5). Biological processes drove the changes in seawater pCO₂, largely on a diel cycle (Fig. 7; Fig. 8). This suggests that carbon sequestration potential of kelp farms in the NGA ~~may beis~~ site-specific. Results from one 360 site cannot be generalized across the region, highlighting the need for studies that compare CO₂ air-sea flux measurements from multiple sites across a heterogenous coastal landscape.

4.1 Influence of site-specific differences in air-sea CO₂ fluxes (FCO₂)

Each site differed in its response to apparent oxygen production, pCO₂ concentration, air-sea CO₂ flux (FCO₂), and periodicity, demonstrating the need to determine site-specific influences on kelp farm carbon uptake (Fig. 3; Fig. 4; Fig. 5; Fig. 6; Fig. 7; 375 Fig. 8). ~~All-Both~~ sites ~~-in the NGA~~ experienced a shift from net heterotrophy to net autotrophy in spring, with a transitional period of a few weeks where the system remained near the O₂ solubility compensation point (Fig. 3). The ~~timing of the~~ shift from heterotrophy to autotrophy ~~in Jakolof Bay occurred a month earlier than a previous study from 2017 analyzing the same bay, though Miller and Kelley (2021) measured seawater 1 m above the seafloor while this study deployed sensors 3 m below the sea surface, suggesting that there may be a delay in shifting from heterotrophy to autotrophy with depth. At two of the three sites (i.e. Kalsin Bay and Windy Bay), the timing of this shift coincided with the ocean changing from a carbon source to a carbon sink (Fig. 4). In contrast, Jakolof Bay became a greater source of carbon to the atmosphere in spring, reaching magnitude fluxes of FCO₂ rarely observed in coastal environments: 2450 mmol·m⁻²·d⁻¹ in Jakolof Bay versus -100 mmol·m⁻²·d⁻¹ in an Arctic lagoon and -131 mmol·m⁻²·d⁻¹ in the Southern California Bight coastal region (Ikawa and Oechel 2015; Miller et al. 2021).~~

380 ~~The elevated biofouling of kelp on the mooring structures in Jakolof Bay may have caused the observed elevated FCO₂ by creating a closed system where the kelp's respiration exceeded its O₂ production. However, synchronous trends in seawater pCO₂ values at the inside and outside moorings in Jakolof Bay suggested that the extreme values measured reflect real conditions (Fig. 4). The exclusion of regular seawater advection near the boundary layer of the sensor electrodes due to the biofouling could drive a wide range of pCO₂ values (Krause-Jensen et al. 2015). The sensors at the other two sites measured a well-mixed water column. However, the O₂ data measured in Jakolof Bay was similar to Kalsin Bay and Windy Bay (Fig. 3), suggesting that the production of O₂ is similar across sites but that the kelp respiration at Jakolof Bay may have been heightened. The respiration rate of kelp will often increase relative to its photosynthetic rate in warmer conditions or with macroalgae-associated microorganisms (Aamot 2011; Kim et al. 2024; Xiong et al. 2024), potentially explaining why seawater pCO₂ in Jakolof Bay became so much higher than the other sites while O₂ remained similar (Fig. 3; Fig. 4). On average, though,~~

385 ~~the FCO₂ flux in the NGA proved similar in magnitude to other coastal locations (Jiang et al. 2013; Ikawa and Oechel 2014; Miller et al. 2021).~~

This study provided the first estimates of air-sea CO₂ fluxes within an Alaskan kelp farm but cannot differentiate between species or population level differences. In ~~Jakolof Bay and~~ Windy Bay, both *S. latissima* and *A. marginata* were grown, while only *A. marginata* was grown in Kalsin Bay. Different kelp species exhibit different rates of photosynthesis due to physiology and diverging adaptations to preferred environment (Van der Loos 2019): *S. latissima* has adapted to low-light and low-energy environments while *A. marginata* has adapted to the high-energy, wave-exposed intertidal. Additionally, intraspecific variation in photosynthetic rates between sites may occur, with regional adaptation to local conditions at these NGA farms that are > 300 km apart (Bruhn et al. 2016).

The farming gear and methods implemented at a given site may also have caused observable differences in the effect of cultured kelp on seawater carbonate chemistry. This study benefitted from studying ~~three-two~~ established commercial kelp farms, but the locations differed in farm size, line spacing, and seeded line source, all of which can influence kelp growth (Boderskov et al. 2021; Lexa Meyer, unpublished). In Kodiak, AK, decreasing the line spacing limited the growth of kelp blades but resulted in higher total yield (Lexa Meyer, unpublished). Notably, the quality of seeded line produced in hatcheries within the NGA varies significantly as these hatcheries continue to improve production for this nascent industry, and seeding method directly correlates with final yields (Boderskov et al. 2021). The variability of farming techniques across locations, paired with site- and species-specific physiology, makes ~~deconvolving-decomposing~~ the primary drivers of kelp production and subsequent FCO₂ difficult to achieve.

4.2 Drivers of nearshore carbonate chemistry in kelp farms

The short-term periodicity observed in seawater $p\text{CO}_2$ was accounted for by diel and tidal cycling, but the longer “event-scale” variability visible in almost all of the timeseries have not yet been explained (Fig. 4; Fig. 78; Fig. 89). Across the sites, this variability spanned 1.6 ~~or 4 to~~ 3.3-day intervals with periodicities strengthening in April and May (Fig. 7). Event-scale variability has previously been attributed to phytoplankton blooms, advection of upwelled water, and wind relaxation (Kapsenberg and Hofmann 2016). Phytoplankton blooms persist on scales of two to three weeks (Eslinger et al. 2001) and wind/air-sea exchange played a minimal role in driving changes in $p\text{CO}_2$ (Fig. 78), so these variables are likely not driving observed periodicity (Fig. 89). Short water residence times in recessed bays in the NGA can cause elevated mixing with offshore water (Haag et al. 2023), and the undersaturated seawater on the continental shelf could act to dilute the inshore $p\text{CO}_2$ with mixing (Evans and Mathis 2013). This mixing with offshore water might explain the event-scale periodicity and remaining residuals from the decomposition of the monthly changes in seawater $p\text{CO}_2$. Windy Bay, in particular, demonstrated elevated residuals from the $p\text{CO}_2$ decomposition, suggesting that our analysis lacked a critical carbon sink at this site. The greatest difference between Windy Bay and ~~the other two sites~~ Kalsin Bay is ~~its~~ the proximity of Windy Bay to the Copper River, the single largest point source of freshwater in the NGA (Reister et al. 2024). While this study is speculative, further research

should quantify the relative carbon fluxes in these bays and determine how long the effect of the carbon uptake by kelp persists in these nearshore sites after harvest.

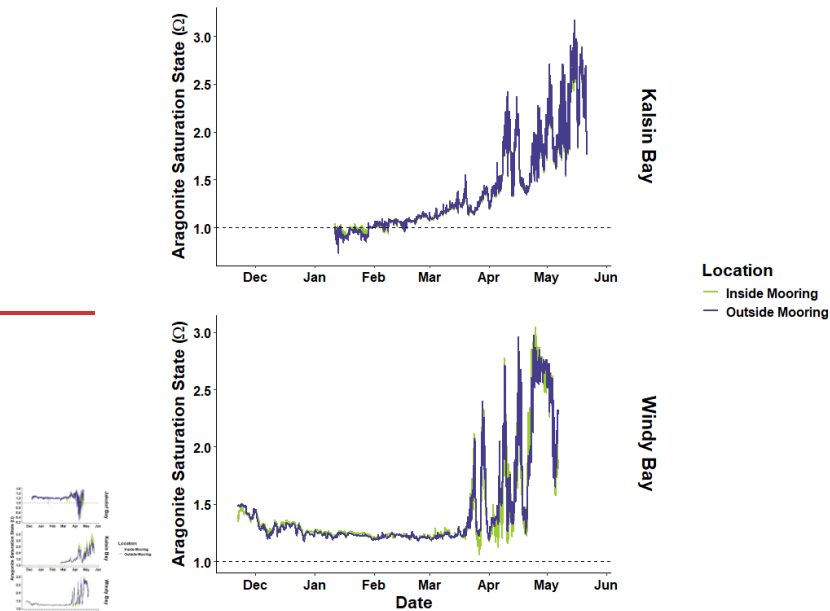
While ~~two-one~~ of the ~~three-two~~ kelp farms provided a net drawdown of atmospheric CO₂ across the growing season, the hourly FCO₂ varied from being a source to a sink of carbon, sometimes within the same twenty-four-hour period (Fig. 5). Coastal oceans exhibit strong diel cycles in pCO₂, and the NGA was not an exception (Fig. 8; Torres et al. 2021). The diel photosynthesis/respiration cycle of primary producers can alter the availability of TA and DIC in seawater, and was the dominant driver of pCO₂ in the region such that it could drive both positive and negative FCO₂ should seawater pCO₂ rise above and fall below atmospheric CO₂ (Fig. 7; Torres et al. 2021). Wind speed dominates the magnitude of these fluxes, therefore an increasing differential between seawater and atmospheric CO₂ would still require strong winds to drive FCO₂ (Eq. 1 and 2). However, wind forcing weakens through spring, which can slow air-sea CO₂ equilibration (Stabeno et al. 2004). Therefore, the timing of wind and air-sea CO₂ differentials are important when considering the ability of kelp farms to draw down atmospheric CO₂, as a mismatch between seasonal winds and the farmed kelp growing season would result in a reduction of CO₂ uptake.

4.3 Carbon credit and ocean acidification mitigation

If one were to consider the uptake of carbon from seawater by a kelp farm, with the assumption that the kelp will be removed from the system through harvest, an estimate of carbon credit capacity can be made using the farm dimensions. The FCO₂ within each farm was fairly homogenous at the timepoint sampled (Fig. 6), further bolstering the notion that the timeseries measured at the mooring was representative of the entire farm. To account for the ability of Alaskan farmed kelps to use CO₂ or bicarbonate as a source of carbon, we calculated the carbon credits two ways: we multiplied both the (1) net integrated dissolved inorganic carbon (DIC) and (2) the net integrated FCO₂ between the inside and outside moorings by the area of the farm assuming the kelp occupied a conservative 1 m depth in the water column. Over the growing season this produced an uptake of DIC into kelp tissue of ~~51,469 tCO₂ eq in Jakolof Bay, 41,151~~ ~~4289~~ tCO₂ eq in ~~Kalsin-Windy Bay, and a release of 6786~~ ~~450~~ tCO₂ eq in ~~Windy-Kalsin Bay, an atmospheric CO₂ drawdown of 27,851~~ ~~tCO₂ eq in Jakolof Bay and 1564~~ ~~4995~~ tCO₂ eq in ~~Kalsin-Windy Bay, and an atmospheric CO₂ release of 69,320~~ ~~286~~ tCO₂ eq in ~~Windy-Kalsin Bay. To sell farmed kelp as a carbon credit, farmers would be required to prevent the harvested biomass from being remineralized by sinking their product off the continental shelf in locations of periodic or permanent anoxia (Pederson et al. 2021; Duarte et al. 2025), or by other means, which would leave the carbon credits as the sole source of income for farmers choosing this route. This method would also remove fixed nutrients from the nearshore system and potentially degrade the marine system (citation), especially if the kelp were grown at scale in this region.~~

Kelp farms may also act as local refugia against ocean acidification by creating a halo effect of lower pH water in their vicinity, altering the seawater chemistry so that biocalcification is more favorable (Krause-Jensen et al. 2015; Ries et al. 2016). When aragonite is ~~in-equilibrium~~ at saturation with respect to seawater, the aragonite saturation state (Ω_{arag}) is 1, and seawater Ω_{arag}

remained above that value across most of the NGA with the exception of late spring in Jakolof Bay (Fig. 9). However, the presence of kelp farms ~~increased~~ reduced the aragonite saturation of seawater in ~~Jakolof Bay and Kalsin-Windy Bay~~ which may ~~decrease~~ increase the exposure of organisms to conditions favouring dissolution in future OA conditions if the kelp farm were to scale up the susceptibility of organisms with calcium carbonate to dissolve, especially during brief windows of opportunity when organisms experience sensitive life stages (Ross et al. 2011). However, in contrast, the ~~Windy-Kalsin Bay~~ kelp farm ~~decreased~~ demonstrated no observable change in aragonite saturation (Fig. 9), indicating that this may not be a universal benefit effect of kelp farms in this region. Another associated benefit could be co-culturing kelp, which increases seawater Ω_{arag} with shellfish. The halo of buffered seawater around a kelp farm would decrease the dissolution of calcifying shellfish and provide a food source to those bivalves as suspended kelp detritus (Haag et al. 2025). Studies have demonstrated that high food availability may alleviate pressures of ocean acidification (Hettinger et al. 2013; Thomsen et al. 2013).



460 **Figure 9:** The aragonite saturation in seawater (Ω_{arag}) inside and outside of kelp farms across the kelp growing season in **Jakolof Bay**, Kalsin Bay, and Windy Bay. The dashed line indicates when seawater is in equilibrium at saturation with respect to aragonite ($\Omega_{\text{arag}} = 1$).

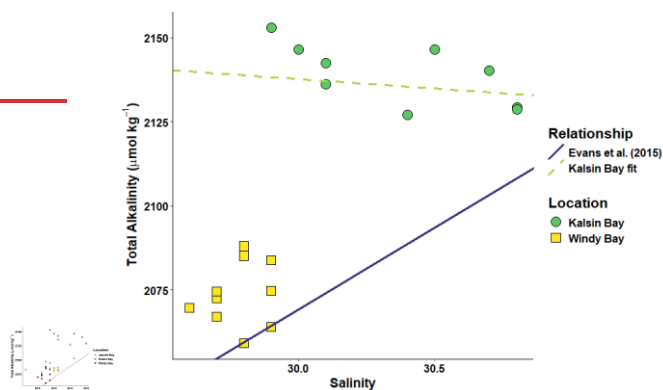
Estimates of other sources and sinks of kelp-derived carbon in the marine environment are needed to contextualize the effect of farmed kelp, particularly the effect of phytoplankton in controlling the seawater carbonate chemistry. There are extended

465 periods of time during summer where farmed kelp is not present, as it is harvested in early spring and not reseeded until the
following winter (Stekoll et al. 2021); however, there are no current estimates in the NGA to the residence time of kelp detritus
in the water column. To ascertain the role of kelp farms in carbon cycling, further research should seek to quantify the longevity
of kelp influence after harvest and natural drivers of carbon in the nearshore. For example, submarine groundwater discharge
plays a dominant role in nutrient cycling in Jakolof Baysouthcentral NGA due to the high tidal forcing in the area (Haag et al.
470 2023)—and tides were also demonstrated to be an important driver of seawater $p\text{CO}_2$ (Fig. 8)—but there are no current
estimates for advective carbon fluxes at the sediment-water interface. Future deployments should pair sensor arrays with
current profilers to more directly resolve tidal advection dynamics as this study could not account for the additional uncertainty
of tidal reversals and with chlorophyll measurements to determine the abundance of phytoplankton in the water column.

5 Conclusions

475 Kelp farms influenced the seawater carbonate chemistry and air-sea CO_2 flux in ~~three-two~~ bays ~~aeross-in~~ the NGA. During the
growing season, which extends from winter into late spring, the farmed kelp at ~~two-one~~ of the ~~three~~ farms increased the capacity
for the nearshore to act as a CO_2 sink, while the ~~third-second~~ farm had the opposite effect. A higher capacity of atmospheric
carbon drawdown may be attainable at targeted farm sites where kelp farms increase the carbon sink capacity of the ocean if
mariculture activities were to scale, though further studies into intraspecific- and interannual variability would be required to
480 actualize a carbon credit market from Alaska's kelp farming industry.

6 Appendix

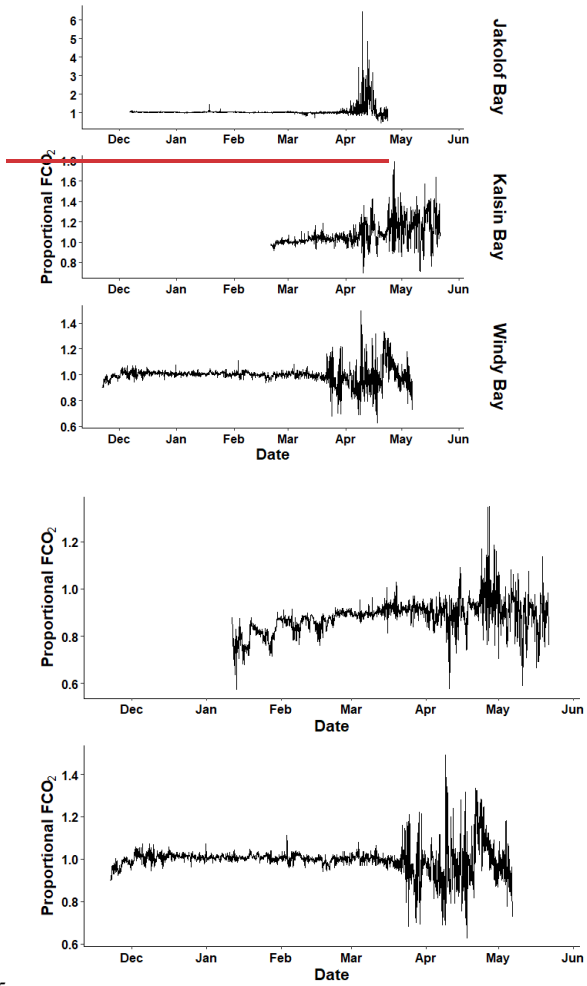


485 **Figure A1.** The spread of discrete samples taken at the farm sites at the end of the sensor deployments (~~April 23 in Jakolof Bay, May 22 in Kalsin Bay, and May 6 in Windy Bay~~) according to their total alkalinity and salinity. Two salinity-temperature relationships are denoted: one he line represents the assumed relationship between total alkalinity and salinity devised by Evans et al. (2015) that was used to convert the salinity timeseries to total alkalinity, and one created specifically for Kalsin Bay using the displayed discrete samples.



490

Figure A2. The biofouled moorings retrieved from Jakolof Bay in spring 2024. Wild-set *Alaria marginata* completely encompassed the mooring frames and sensors.



495

Figure A23. The proportional difference in air-sea CO₂ fluxes (FCO₂) between the inside of a kelp farm relative to ambient conditions at three different sites calculated by dividing the inside mooring by the outside mooring.

6.1 TA-salinity sensitivity analysis

We adapted the methods of Fassbender et al. (2017) to estimate the sensitivity of $p\text{CO}_2$ values derived from predicted total alkalinity (TA) values. The sensor arrays deployed in this study did not measure TA, so we wanted to use a known salinity-TA relationship established by Evans et al. (2015) for the region to estimate a timeseries of TA to then estimate $p\text{CO}_2$ as estimations of the carbonate system require two known variables. We utilized discrete samples measured for TA and one other carbonate chemistry parameter in the lab for this purpose. First, we predicted the TA values for the bottle samples only using salinity and the Evans et al. (2015) relationship. Next, we calculated the residual for the bottle samples predicted TA and the measured TA. Then, we used the 'seacarb' package in R to estimate the $p\text{CO}_2$ for each sample twice, once using the predicted TA and once the measured TA, and compared again the final $p\text{CO}_2$ values for the sensitivity. The results demonstrated that the Evans et al. (2015) relationship would work for one of the two sites only (Table A1).

Table A1. The residuals associated with the difference between the measured total alkalinity and resulting estimated $p\text{CO}_2$ value and a total alkalinity value predicted by Evans et al. (2015) and its resulting estimated $p\text{CO}_2$ value. Values are shown as the mean \pm standard deviation.

Location	TA residual ($\mu\text{mol kg}^{-1}$)	$p\text{CO}_2$ residual (μatm)
Windy Bay	-15.22 ± 9.85	3.76 ± 2.47
Kalsin Bay	-51.65 ± 24.32	-140.53 ± 58.49

We calculated a site-specific salinity-TA relationship for Kalsin Bay as the Evans et al. (2015) relationship massively underestimated the resulting $p\text{CO}_2$ values (Table A1). Using 6 of the 9 discrete bottle samples, a linear model was created:

$$\text{Total alkalinity} = \text{Salinity} * (-5.613) + 2306.137 \quad (A1)$$

The last 3 discrete samples were treated the same as above, and the final residual for $p\text{CO}_2$ demonstrated a much better match than the Evans et al. (2015) relationship (Table A2).

Table A2. The residuals associated with the difference between the measured total alkalinity and resulting estimated $p\text{CO}_2$ value and a total alkalinity value predicted by Equation A1 and its resulting estimated $p\text{CO}_2$ value. Values are shown as the mean \pm standard deviation.

Location	TA residual ($\mu\text{mol kg}^{-1}$)	$p\text{CO}_2$ residual (μatm)
Kalsin Bay	-9.62 ± 4.74	-15.40 ± 6.79

7 Code availability

The code utilized in this project was minorly modified from pre-existing packages or code already publicly available, so it has not been published anywhere.

8 Data availability

Data can be accessed from the DataONE repository (<https://doi.org/10.24431/rw1k9hb>).

Formatted: Font: 10 pt, Not Bold

Formatted: Font: 10 pt, Not Bold, Italic

Formatted: Font: 10 pt, Not Bold

Formatted: Font: 10 pt, Not Bold, Subscript

Formatted: Font: 10 pt, Not Bold

Formatted: Space Before: 6 pt, After: 6 pt, Line spacing 1.5 lines

Formatted: Font: 10 pt, Not Bold, Italic

Formatted: Font: 10 pt, Not Bold

Formatted: Font: 10 pt, Not Bold, Subscript

Formatted: Font: 10 pt, Not Bold

Formatted: Font: 10 pt, Not Bold, Italic

Formatted: Font: 10 pt, Not Bold

Formatted: Font: 10 pt, Not Bold, Subscript

Formatted: Font: 10 pt, Not Bold

Formatted: Font: 10 pt, Not Bold, Italic

Formatted: Font: 10 pt, Not Bold

Formatted: Font: 10 pt, Not Bold, Subscript

Formatted: Font: 10 pt, Not Bold

Formatted: Font: Italic

Formatted: Subscript

Formatted: Line spacing: single

Formatted: Font: Italic

Formatted: Subscript

Formatted: Font: Italic

Formatted: Subscript

Formatted: Font: Italic

Formatted: Subscript

Formatted: English (Canada)

Formatted: Line spacing: single

Formatted: Space Before: 6 pt, After: 6 pt, Line spacing 1.5 lines

9 Author contribution

AK acquired the funding and designed the project with JH. The investigation and data processing was conducted by JH, AK, and JJ. Formal analysis and writing of the original draft was conducted by JH with aid from AK and CM. All authors contributed to the reviewing and editing of the manuscript.

530 10 Competing interests

The authors declare that they have no conflict of interest.

11 Acknowledgments

535 Samples were collected on the unceded traditional homelands of the Dena'ina, Alutiiq, Eyak, and Sugpiaq and samples were processed on the unceded traditional homelands of the Lower Tanana Dené. Thank you to the kelp farmers who worked with us: Lindsay Olsen and Larry Lansdowne of Spinnaker Sea Farms, Alf Pryor and Lexa Meyer of Alaska Ocean Farms, and Thea Thomas and Cale Herschleb of Royal Ocean Kelp Co. Thank you to Dr. Sarah Mincks, Marina Alcantar, Jonah Jossart, Alorah Bliese, and Emily Ortega for aid in sample collection/processing, data analysis, and manuscript edits. This research was financially supported by the Rasmuson Fisheries Research Center, the Exxon Valdez Oil Spill Mariculture Research and Restoration Consortium, and the Northern Gulf of Alaska Applied Research Award.

540 12 References

- Aamot, I. A.: *How photosynthesis in Laminaria digitata and Saccharina latissima is affected by water temperature* MSc thesis, Institutt for biologi, Norwegian University of Science and Technology. <http://hdl.handle.net/11250/244793>, 2011.
- Alcantar, M. W., Hetrick, J., Ramsay, J., and Kelley, A. L.: Examining the impacts of elevated, variable $p\text{CO}_2$ on larval Pacific razor clams (*Siliqua patula*) in Alaska, F. in Mar. Sci., 11, 1253702, doi:[10.3389/fmars.2024.1253702](https://doi.org/10.3389/fmars.2024.1253702), 2024.
- 545 Arzeno-Soltero, I. B., Saenz, B. T., Frieder, C. A., Long, M. C., DeAngelo, J., Davis, S. J., and Davis, K. A.: Large global variations in the carbon dioxide removal potential of seaweed farming due to biophysical constraints, Com. Ear. Env., 4, 185, doi:[10.1038/s43247-023-00833-2](https://doi.org/10.1038/s43247-023-00833-2), 2023.
- Bignami, S., Sponaugle, S., and Cowen, R. K.: Response to ocean acidification in larvae of a large tropical marine fish, *Rachycentron canadum*. Glob. Cha. Bio., 19(4), 996-1006, doi:[10.1111/gcb.12133](https://doi.org/10.1111/gcb.12133), 2023.
- 550 Boderskov, T., Nielsen, M. M., Rasmussen, M. B., Balsby, T. J. S., Macleod, A., Holdt, S. L., Sloth, J.J., and Bruhn, A.: Effects of seeding method, timing and site selection on the production and quality of sugar kelp, *Saccharina latissima*: A Danish case study, Alg. Res., 53, 102160, doi:[10.1016/j.algal.2020.102160](https://doi.org/10.1016/j.algal.2020.102160), 2021.
- Bresnahan Jr, P. J., Martz, T. R., Takeshita, Y., Johnson, K. S., and LaShomb, M.: Best practices for autonomous measurement of seawater pH with the Honeywell Durafet, Meth. in Oce., 9, 44-60, doi:[10.1016/j.mio.2014.08.003](https://doi.org/10.1016/j.mio.2014.08.003), 2014.

- 555 Bruhn, A., Tørring, D. B., Thomsen, M., Canal-Vergés, P., Nielsen, M. M., Rasmussen, M. B., Eybye K.L., Larsen, M.M., Balsby, T.J.SI, and Petersen, J. K.: Impact of environmental conditions on biomass yield, quality, and bio-mitigation capacity of *Saccharina latissima*, *Aqu. Env. Inter.*, 8, 619-636, doi:[10.3354/aci00200](https://doi.org/10.3354/aci00200), 2016.
- Bullen, C. D., Driscoll, J., Burt, J., Stephens, T., Hessing-Lewis, M., and Gregr, E. J.: The potential climate benefits of seaweed farming in temperate waters, *Sci. Rep.*, 14(1), 15021, doi:[10.1038/s41598-024-65408-3](https://doi.org/10.1038/s41598-024-65408-3), 2024.
- 560 Cai, W. J.: Estuarine and coastal ocean carbon paradox: CO₂ sinks or sites of terrestrial carbon incineration?, *Ann. Rev. of Mar. Sci.*, 3(1), 123-145, doi:[10.1146/annurev-marine-120709-142723](https://doi.org/10.1146/annurev-marine-120709-142723), 2011.
- Casamitjana, X., and Roget, E.: Resuspension of sediment by focused groundwater in Lake Banyoles. *Limn. and Oce.*, 38(3), 643-656, doi:[10.4319/lo.1993.38.3.0643](https://doi.org/10.4319/lo.1993.38.3.0643), 1993.
- Chen, C. T. A., and Borges, A. V.: Reconciling opposing views on carbon cycling in the coastal ocean: Continental shelves as sinks and near-shore ecosystems as sources of atmospheric CO₂, *Deep Sea Res. Part II: Top. Stud. in Oce.*, 56(8-10), 578-590, doi:[10.1016/j.dsr2.2009.01.001](https://doi.org/10.1016/j.dsr2.2009.01.001), 2009.
- 565 Coleman, S., Dewhurst, T., Fredriksson, D. W., St. Gelais, A. T., Cole, K. L., MacNicol, M., Laufer, E., and Brady, D. C.: Quantifying baseline costs and cataloging potential optimization strategies for kelp aquaculture carbon dioxide removal, *Front. in Mar. Sci.*, 9, 966304, doi:[10.3389/fmars.2022.966304](https://doi.org/10.3389/fmars.2022.966304), 2022.
- 570 DeAngelo, J., Saenz, B. T., Arzeno-Soltero, I. B., Frieder, C. A., Long, M. C., Hamman, J., Davis, K. A., and Davis, S. J.: Economic and biophysical limits to seaweed farming for climate change mitigation, *Nat. Pla.*, 9(1), 45-57, doi:[10.1038/s41477-022-01305-9](https://doi.org/10.1038/s41477-022-01305-9), 2023.
- Douglas, N. K., and Byrne, R. H.: Achieving accurate spectrophotometric pH measurements using unpurified meta-cresol purple, *Mar. Chem.*, 190, 66-72, doi:[10.1016/j.marchem.2017.02.004](https://doi.org/10.1016/j.marchem.2017.02.004), 2017.
- 575 Duarte, C. M., Delgado-Huertas, A., Marti, E., Gasser, B., Martin, I. S., Cousteau, A., Neumeyer, F., Reilly-Cayten, M., Boyce, J., Kuwae, T., Hori, M., Miyajima, T., Price, N. N., Arnold, S., Ricart, A. M., Davis, S., Surugau, N., Abdul, A., Wu, J., Chung, I. K., Choi, C. G., Sondak, C. F. A., Albasri, H., Krause-Jensen, D., Bruhn, A., Boderskov, T., Hancke, K., Funderud, J., Borrero-Santiago, A. R., Pascal, F., Joanne, P., Ranivoarivelo, L., Collins, W. T., Clark, J., Gutierrez, J. F., Riquelme, R., Avila, M., Macreadie, P. I., and Masque, P.: Carbon burial in sediments below seaweed farms matches that of Blue Carbon habitats, *Nat. Cli. Cha.*, 1-8, doi:[10.1038/s41558-025-02278-1](https://doi.org/10.1038/s41558-025-02278-1), 2025.
- 580 Edgar, G. J., Bates, A. E., Krueck, N. C., Baker, S. C., Stuart-Smith, R. D., and Brown, C. J.: Stock assessment models overstate sustainability of the world's fisheries, *Sci.*, 385(6711), 860-865, doi:[10.1126/science.adl6282](https://doi.org/10.1126/science.adl6282), 2024.

- Eslinger, D. L., Cooney, R. T., Mcroy, C. P., Ward, A., Kline Jr, T. C., Simpson, E. P., Wang, J., and Allen, J. R.: Plankton dynamics: observed and modelled responses to physical conditions in Prince William Sound, Alaska, *Fish. Oce.*, 10, 81-96, doi:[10.1046/j.1054-6006.2001.00036.x](https://doi.org/10.1046/j.1054-6006.2001.00036.x), 2001.
- 585 Evans, W., and Mathis, J. T.: The Gulf of Alaska coastal ocean as an atmospheric CO₂ sink, *Con. S. Res.*, 65, 52-63, doi:[10.1016/j.csr.2013.06.013](https://doi.org/10.1016/j.csr.2013.06.013), 2013.
- Evans, W., Mathis, J. T., Ramsay, J., and Hetrick, J. On the frontline: Tracking ocean acidification in an Alaskan shellfish hatchery, *P. One*, 10(7), e0130384, doi:[10.1371/journal.pone.0130384](https://doi.org/10.1371/journal.pone.0130384), 2015.
- 590 Fassbender, A. J., Alin, S. R., Feely, R. A., Sutton, A. J., Newton, J. A., and Byrne, R. H.: Estimating total alkalinity in the Washington State coastal zone: complexities and surprising utility for ocean acidification research, *Est. and Coas.*, 40(2), 404-418, 2017.
- Feely, R. A., Sabine, C. L., Lee, K., Berelson, W., Kleypas, J., Fabry, V. J., and Millero, F. J.: Impact of anthropogenic CO₂ on the CaCO₃ system in the oceans, *Sci.*, 305(5682), 362-366, doi:[10.1126/science.1097329](https://doi.org/10.1126/science.1097329), 2004.
- 595 Gattuso, J.P., Epitalon, J.M., Lavigne, H., Orr, J., Gentili, B., Hagens, M., Hofmann, A., Mueller, J.D., Proye, A., Rae, J. and Soetaert, K.: Package 'seacarb'. doi:10.32614/CRAN.package.seacarb, 2015.
- Gattuso, J.P., Epitalon, J.M., Lavigne, H., Orr, J., Gentili, B., Hagens, M., Hofmann, A., Mueller, J.D., Proye, A., Rae, J. and Soetaert, K., 2015. Package 'seacarb'. *Preprint at <http://cran.r-project.org/package=seacarb>*.
- Garcia, H. E., and Gordon, L. I.: Oxygen solubility in seawater: Better fitting equations, *Lim. and Oce.*, 37(6), 1307-1312, doi:[10.4319/lo.1992.37.6.1307](https://doi.org/10.4319/lo.1992.37.6.1307), 1992.
- 600 García-Troche, E. M., Morell, J. M., Meléndez, M., and Salisbury, J. E.: Carbonate chemistry seasonality in a tropical mangrove lagoon in La Parguera, Puerto Rico, *P. One*, 16(5), e0250069, doi:[10.1371/journal.pone.0250069](https://doi.org/10.1371/journal.pone.0250069), 2021.
- Haag, J., Dulai, H., and Burt, W.: The role of submarine groundwater discharge to the input of macronutrients within a macrotidal subpolar estuary, *Est. and Coa.*, 46(7), 1740-1755, doi:10.1007/s12237-023-01231-9, 2023.
- 605 Haag, J., Mincks, S. L., Jossart, J., and Kelley, A. L.: Seasonal trophic resource partitioning by Pacific oyster *Crassostrea gigas* and Pacific blue mussel *Mytilus trossulus* in an Alaskan estuary, *Mar. Eco. Prog. Ser.*, 754, 65-76, doi:[10.3354/meps14779](https://doi.org/10.3354/meps14779), 2025.
- Hettinger, A., Sanford, E., Hill, T. M., Hosfelt, J. D., Russell, A. D., and Gaylord, B.: The influence of food supply on the response of Olympia oyster larvae to ocean acidification, *Biogeosci.*, 10(10), 6629-6638, doi:10.5194/bg-10-6629-2013, 2013.
- 610 Ikawa, H., and Oechel, W. C. Temporal variations in air-sea CO₂ exchange near large kelp beds near San Diego, California, *Jou. of Geophys. Res.: Oce.*, 120(1), 50-63, doi:[10.1002/2014JC010229](https://doi.org/10.1002/2014JC010229), 2015.

Formatted: Font: Not Italic

Formatted: Font: Not Italic

- IPCC.: *Climate Change 2022: Impacts, Adaptation, and Vulnerability*. Contribution of Working Group II to the Sixth Assessment Report of the Intergovernmental Panel on Climate Change, Cambridge University Press, Cambridge, UK and New York, NY, USA, doi:[10.1017/9781009325844](https://doi.org/10.1017/9781009325844), 2022.
- 615 Jiang, Z., Fang, J., Mao, Y., Han, T., and Wang, G.: Influence of seaweed aquaculture on marine inorganic carbon dynamics and sea-air CO₂ flux, *Jou. of the Wor. Aqu. Soc.*, 44(1), 133-140, doi:[10.1111/jwas.12000](https://doi.org/10.1111/jwas.12000), 2013.
- Jiang, Z., Li, J., Qiao, X., Wang, G., Bian, D., Jiang, X., Liu, Y., Huang, D., Wang, W., and Fang, J.: The budget of dissolved inorganic carbon in the shellfish and seaweed integrated mariculture area of Sanggou Bay, Shandong, China, *Aqua.*, 446, 167-174, doi:[10.1016/j.aquaculture.2014.12.043](https://doi.org/10.1016/j.aquaculture.2014.12.043), 2015.
- 620 Kaiser, D. Davidatlarge/ggTS: ggTS first release (v1.0.0). Zenodo, doi:[10.5281/zenodo.3901308](https://doi.org/10.5281/zenodo.3901308), 2020.
- Kapsenberg, L., and Hofmann, G. E.: Ocean pH time-series and drivers of variability along the northern Channel Islands, California, USA. *Limn. and Oce.*, 61(3), 953-968, doi:[10.1002/lno.10264](https://doi.org/10.1002/lno.10264), 2016.
- Kelley D., Richards C., and SCOR/IAPSO W.: `_gsw: Gibbs Sea Water Functions` . R package version 1.2-0, https://CRAN.R-project.org/package=_gsw, 2024.
- 625 Kim, J. H., Moon, H., Han, M. J., Jung, J. E., Lee, N. Y., Kang, J. W., Oh, J. C., Park, G., Lee, S., Lee, M., Park, C., Yoon, H., and Kim, H. The photosynthetic uptake of inorganic carbon from *Pyropia seaweed* aquaculture beds: Scaling up population-level estimations, *Aqua.*, 593, 741293, doi: [10.1016/j.aquaculture.2024.741293](https://doi.org/10.1016/j.aquaculture.2024.741293), 2024.
- Krause-Jensen, D., Duarte, C. M., Hendriks, I. E., Meire, L., Blicher, M. E., Marbà, N., and Sejr, M. K.: Macroalgae contribute to nested mosaics of pH variability in a subarctic fjord. *Biogeosci.*, 12(16), 4895-4911, doi:10.5194/bg-12-4895-2015, 2015.
- 630 Kurihara, H., Yin, R., Nishihara, G. N., Soyano, K., and Ishimatsu, A.: Effect of ocean acidification on growth, gonad development and physiology of the sea urchin *Hemicentrotus pulcherrimus*. *Aqu. Bio.*, 18(3), 281-292, doi:[10.3354/ab](https://doi.org/10.3354/ab), 2013.
- Lewis, E. R., and Wallace, D. W. R.: Program developed for CO₂ system calculations. Environmental System Science Data Infrastructure for a Virtual Ecosystem (ESS-DIVE)(United States), doi: [10.15485/1464255](https://doi.org/10.15485/1464255), 1998.
- Ligges, U., Short, T., Kienzle, P., Schnackenberg, S., Billinghamurst, D., Borchers, H.W., Carezia, A., Dupuis, P., Eaton, J.W.,
635 Farhi, E., Habel, K., Hornik, K., Krey, S., Lash, B., Leisch, F., Mersmann, O., Neis, P., Ruohio, J., Smith III, J. O., Stewart, D., Weingessel, A.: Package 'signal'. R Found. for Stat. Comp., doi:10.32614/CRAN.package.signal, 2015.
- Long, W. C., Swiney, K. M., and Foy, R. J.: Effects of ocean acidification on the embryos and larvae of red king crab, *Paralithodes camtschaticus*. *Mar. Poll. Bull.*, 69(1-2), 38-47, doi:[10.1016/j.marpolbul.2013.01.011](https://doi.org/10.1016/j.marpolbul.2013.01.011), 2013.
- MacIntyre, S.: Trace gas exchange across the air-sea interface in fresh water and coastal marine environments. *Biogen. Tr.*
640 Gases: Meas. Emi. From S. And W., 52-97, <https://cir.nii.ac.jp/crid/1571698600697327104>, 1995.

McKain, K., Sweeney, C., Baier, B., Crotwell, A., Crotwell, M., Handley, P., Higgs, J., Legard, T., Madronich, M., Miller, J. B., Moglia, E., Mund, J., Newberger, T., Wolter, S., and NOAA Global Monitoring Laboratory.: NOAA Global Greenhouse Gas Reference Network Flask-Air PFP Sample Measurements of CO₂, CH₄, CO, N₂O, H₂, SF₆ and isotopic ratios collected from aircraft vertical profiles [Data set]. Version: 2024-08-12. doi:[10.15138/39HR-9N34](https://doi.org/10.15138/39HR-9N34), (Accessed 12/6/2024).

645 Miller, C. A., Pocock, K., Evans, W., and Kelley, A. L.: An evaluation of the performance of Sea-Bird Scientific's SeaFET™ autonomous pH sensor: considerations for the broader oceanographic community. *Oce. Sci.*, 14(4), 751-768, doi:10.5194/os-14-751-2018, 2018.

Miller, L.: Legalizing local: Alaska's unique opportunity to create an equitable and sustainable seaweed farming industry. *Alaska L. Rev.*, 38, 313-340, 2021.

650 Miller, C. A., Bonsell, C., McTigue, N. D., and Kelley, A. L.: The seasonal phases of an Arctic lagoon reveal the discontinuities of pH variability and CO₂ flux at the air–sea interface. *Biogeosci.*, 18(3), 1203-1221, doi:10.5194/bg-18-1203-2021, 2021.

Miller, C. A., and Kelley, A. L.: Seasonality and biological forcing modify the diel frequency of nearshore pH extremes in a subarctic Alaskan estuary. *Limn. and Oce.*, 66(4), 1475-1491, doi:[10.1002/lno.11698](https://doi.org/10.1002/lno.11698), 2021.

655 [National Academy of Sciences, Engineering, and Medicine: A research strategy for ocean-based carbon dioxide removal and sequestration. Washington, DC: Natl. Acad. Press, 2021.](#)

NOAA National Wind Buoy. <https://www.ndbc.noaa.gov/>, (Accessed 12/26/2024)

Mongin, M., Baird, M. E., Hadley, S., and Lenton, A.: Optimising reef-scale CO₂ removal by seaweed to buffer ocean acidification. *Env. Res. Let.*, 11(3), 034023, doi:10.1088/1748-9326/11/3/034023, 2016.

660 Oschlies, A., Bach, L. T., Fennel, K., Gattuso, J. P., and Mengis, N.: Perspectives and challenges of marine carbon dioxide removal. *Front. in Cli.*, 6, 1506181, doi:[10.3389/fclim.2024.1506181](https://doi.org/10.3389/fclim.2024.1506181), 2025.

Pedersen, M. F., Filbee-Dexter, K., Frisk, N. L., Sárosy, Z., and Wernberg, T.: Carbon sequestration potential increased by incomplete anaerobic decomposition of kelp detritus. *Mar. Eco. Prog. Ser.*, 660, 53-67, doi:<https://doi.org/10.3354/meps>, 2021.

665 Quéré, C., Andrew, R. M., Friedlingstein, P., Sitch, S., Hauck, J., Pongratz, J., Pickers, P. A., Korsbakken, J. I., Peters, G. P., Canadell, J. G., Arneeth, A., Chevallier, F., Chini, L. P., Ciais, P., Doney, S. C., Gkritzalis, T., Goll, D. S., Harris, I., Haverd, V., Hoffman, F. M., Hoppema, M., Houghton, R. A., Hurtt, G., Ilyina, T., Jain, A. K., Johannessen, T., Jones, C. D., Kato, E., Keeling, R. F., Goldewijk, K. K., Landschützer, P., Lefèvre, N., Lienert, S., Liu, Z., Lombardozi, D., Metzl, N., Munro, D. R., Nabel, J. E. M. S., Nakaoka, S., Neill, C., Olsen, A., Ono, T., Patra, P., Peregón, A., Peters, W., Peylin, P., Pfeil, B., Pierrot, D., Poulter, B., Rehder, G., Resplandy, L., Robertson, E., Rocher, M., Rödenbeck, C., Schuster, U., Schwinger, J., Séférian, R., Skjelvan, I., Steinhoff, T., Sutton, A., Tans, P. P., Tian, H., Tilbrook, B., Tubiello, F. N., van der Laan-Luijkx, I. T., van

Formatted: Font: Not Italic

- der Werf, G. R., Viovy, N., Walker, A. P., Wiltshire, A. J., Wright, R., Zaehle, S., and Zheng, B.: Global carbon budget 2018, *Ear. Sys. Sci. Data.*, 10, 2141-2194, doi:10.5194/essd-10-2141-2018, 2018.
- Reister, I., Danielson, S., and Aguilar-Islas, A.: Perspectives on Northern Gulf of Alaska salinity field structure, freshwater pathways, and controlling mechanisms, *Prog. in Occ.*, 103373, doi:10.1016/j.poccean.2024.103373, 2024.
- 675 Ries, J. B., Ghazaleh, M. N., Connolly, B., Westfield, I., and Castillo, K. D.: Impacts of seawater saturation state ($\Omega_A = 0.4-4.6$) and temperature (10, 25 C) on the dissolution kinetics of whole-shell biogenic carbonates, *Geochim. et Cosmochim. Acta.*, 192, 318-337, doi:10.1016/j.gca.2016.07.001, 2016.
- Ross, P. M., Parker, L., O'Connor, W. A., and Bailey, E. A.: The impact of ocean acidification on reproduction, early development and settlement of marine organisms, *Wat.*, 15(11), doi:10.3390/w3041005, 2011.
- 680 Stabeno, P. J., Bond, N. A., Hermann, A. J., Kachel, N. B., Mordy, C. W., and Overland, J. E.: Meteorology and oceanography of the Northern Gulf of Alaska, *Cont. Shelf Res.*, 24(7-8), 859-897, doi:10.1016/j.csr.2004.02.007, 2004.
- Stekoll, M. S., Peeples, T. N., and Raymond, A. E.: Mariculture research of *Macrocystis pyrifera* and *Saccharina latissima* in Southeast Alaska, *Jour. of the Wor. Aqua. Soc.*, 52(5), 1031-1046, doi:10.1111/jwas.12765, 2021.
- Thomsen, J., Casties, I., Pansch, C., Körtzinger, A., and Melzner, F.: Food availability outweighs ocean acidification effects in juvenile *Mytilus edulis*: laboratory and field experiments, *Glob. Cha. Bio.*, 19(4), 1017-1027, doi:10.1111/gcb.12109, 2013.
- 685 Torres, O., Kwiatkowski, L., Sutton, A. J., Dorey, N., and Orr, J. C.: Characterizing mean and extreme diurnal variability of ocean CO₂ system variables across marine environments, *Geophys. Res. Lett.* 48(5), e2020GL090228, doi:10.1029/2020GL090228, 2021.
- Trapletti, A., Hornik, K., LeBaron, B., and Hornik, M. K.: Package 'tseries'. R proj. doi: 10.32614/CRAN.package.tseries, 690 2015.
- John, C. R., and Watson, D.: Spectrum: Fast Adaptive Spectral Clustering for Single and Multi-View Data, doi: 10.32614/CRAN.package.Spectrum, 2020.
- van der Loos, L. M., Schmid, M., Leal, P. P., McGraw, C. M., Britton, D., Revill, A. T., Virtue, P., Nichols, P. D., and Hurd, C. L.: Responses of macroalgae to CO₂ enrichment cannot be inferred solely from their inorganic carbon uptake strategy. *Eco. and Evol.*, 9(1), 125-140, doi:10.1002/ece3.4679, 2019.
- 695 Wanninkhof, R. Relationship between wind speed and gas exchange over the ocean revisited. *Limn. and Oce.: Met.*, 12(6), 351-362, doi:10.1029/92JC00188, 2014.
- Williams, C. R., Dittman, A. H., McElhany, P., Busch, D. S., Maher, M. T., Bammler, T. K., MacDonald, J. W., and Gallagher, E. P.: Elevated CO₂ impairs olfactory-mediated neural and behavioral responses and gene expression in ocean-phase coho salmon (*Oncorhynchus kisutch*), *Glob. Cha. Bio.*, 25(3), 963-977, doi:10.1111/gcb.14532, 2019.
- 700

Xiong, T., Li, H., Hu, Y., Zhai, W. D., Zhang, Z., Liu, Y., Zhang, J., Lu, L., Chang, L., Xe, L., Wei, Q., Jiao, N., and Zhang, Y.: Seaweed farming environments do not always function as CO₂ sink under synergistic influence of macroalgae and microorganisms. *Agr., Eco. & Env.*, 361, 108824, doi:[10.1016/j.agee.2023.108824](https://doi.org/10.1016/j.agee.2023.108824), 2024.